Transactions, SMiRT-22
San Francisco, California, USA - August 18-23, 2013
Division IX (include assigned division number from I to X)

MACRO AND MICRO RESIDUAL STRESSES IN ZIRCONIUM OXIDE LAYERS

Serge PASCAL[1,2], Clotilde BERDIN[3] and Zhao Yue YAO[1,3]

[1] CEA, DEN, DM2S, SEMT, CEA Saclay, F-91191 Gif-sur-Yvette, France
[2] LaMSID, UMR CNRS-EDF-CEA 8193, F-92141 Clamart, France
[3] Univ. Paris-Sud, LEMHE- ICMMO, CNRS UMR 8182, F-91405 Orsay cedex, France

ABSTRACT

The aim of this work is to study the influence of crystallographic and morphological textures on the evaluation of the residual stresses in zirconium oxide layers by finite element computations. This is studied for thermal stresses at two scales: at a macroscopic scale to obtain the first residual stresses order and at a microscopic scale in order to obtain second residual stresses order, *i.e.* the intragranular stresses, but also to assess the equivalent behavior of the polycrystalline oxide by homogenization procedures. The results show that for thin layers: 1) the analytical formulas commonly used to derive the residual stresses from strain measurements can be used if the assumptions on the thermo-elastic properties of the oxide layer are correct; 2) computations on polycrystalline aggregates of zirconia give better assessments of the thermo-elastic properties of the polycrystalline oxide and showed that there is no influence of the morphological texture; 3) a large spread in intragranular stress distribution can be observed in the layer; this stress level should be integrated to the failure analysis of the zirconium oxide layers.

INTRODUCTION

Residual stresses are generally derived from experimental strain measurements through analytical calculations; see Benali et al. (2006), Bernard et al. (2007), and Chen et al. (2011). These calculations rely on assumptions upon the mechanical characteristics of the oxide layers, in particular their isotropy. However, their microstructures are usually characterized by morphological and crystallographic textures. The aim of this work is to study the influence of some microstructural parameters on the evaluation of the residual stresses in zirconium oxide layers by finite element computations. In a first attempt, only thermal stresses are taken into account.

The influence of the oxide layer microstructure is studied at two scales. At the oxide/substrate system scale, the oxide layer is viewed as a homogenous media but with thermo-elastic properties derived from its polycrystalline microstructure. Each grain of the polycrystal is assumed to be monoclinic zirconia since this is the phase mostly developed during the oxidation of zirconium. Two distributions of crystalline orientations are considered for the polycrystalline aggregate: the isotropic distribution and one ideal fiber texture. The thermo-elastic properties of these microstructures are obtained thanks to the Voigt and Reuss bounds. Finally, these properties are used into finite element analyses of the stresses developed in the layer/substrate system during thermal loading.

At the microstructural scale, we study the influence of the morphological and crystallographic textures of the oxide layers by performing finite element analyses of Volume Elements of polycrystalline aggregates. Volume Elements with equiaxed grains are modeled by Voronoï polyhedrons, each grain behaving as monoclinic. The effective thermo-elastic properties of these VE are computed and compared to the Voigt and Reuss bounds. Moreover, intra-granular stress distributions are also presented to show that the stress level may locally be much higher than its mean value in the layer.

In the following, we first present the material data used for the simulations as well as the Voigt and Reuss bounds used to estimate the thermo-elastic properties of the polycrystalline oxide layer. In the next part, we detail the analyses achieved at the macro scale, presenting the Finite Element (FE) model

used to compute the stress state induced by thermal loading. It is worth noting that the growth stresses can be computed as the thermal stresses. The stress level computed in the oxide layer is then compared to the usual estimates given by analytical calculations, considering elastic behavior for the layer as well as for the substrate. Assumptions made to achieve the analyses at the macro scale are then discussed in the analysis at the micro scale. The effective properties of the different investigated crystallographic distributions are computed by FE simulations on polycrystalline aggregates and compared to the Voigt and Reuss estimates. Finally, we present the intra-granular stress distribution in the oxide layer according to different crystallographic textures and different grain morphology. The last part of this article sums up the main results and presents the ongoing studies.

MATERIAL DATA AND PROCEDURE

Thermo-Elastic Properties of Monoclinic Zirconia

Monoclinic zirconia, ZrO2m, is characterized by the following lattice parameters: a=0.508 nm, b=0.521 nm and c=0.531 nm with an angle β=99.23° defined by $\cos\beta = \vec{e}_a.\vec{e}_c$ (see Parise et al. (1998), and Zhao et al. (2011)) where $\vec{e}_a$, $\vec{e}_c$ are the unit vectors along the a and c axes, respectively. The crystallographic frame is then $(\vec{e}_a, \vec{e}_b, \vec{e}_c)$. The mechanical behavior of the monoclinic zirconia crystal is anisotropic. It is generally expressed in the crystallophysic frame $(\vec{c}_1, \vec{c}_2, \vec{c}_3)$ defined by Equation 1. Equation 2 gives the moduli tensor expressed in this frame using the Voigt notation ($C_{44}=C_{1212}$, $C_{66}=C_{2323}$), see Parise et al. (1998), Zhao et al. (2011), and Berdin et al. (2013). The thermal expansion coefficients are α_{aa}=7.16 10^{-6} K^{-1}, α_{bb}=2.16 10^{-6} K^{-1} and α_{cc}=12.6 10^{-6} K^{-1}, see Simeone et al. (2003).

$$\vec{a} = \vec{c}_1 \sin\beta + \vec{c}_3 \cos\beta\,,\ \vec{b} = \vec{c}_2,\ \vec{c} = \vec{c}_3 \tag{1}$$

$$C_{IJ}{}^{c}(\mathrm{GPa}) = \begin{pmatrix} 358 & 144 & 67 & 0 & -25.9 & 0 \\ 144 & 426 & 127 & 0 & 38.3 & 0 \\ 67 & 127 & 240 & 0 & -23.3 & 0 \\ 0 & 0 & 0 & 130 & 0 & 38.8 \\ -25.9 & 38.3 & -23.3 & 0 & 78.7 & 0 \\ 0 & 0 & 0 & 38.8 & 0 & 99.1 \end{pmatrix} \tag{2}$$

As can be seen, monoclinic zirconia is highly anisotropic with C_{22}/C_{33}=1.77 and α_{cc}/α_{bb}=6. In the following, two distributions of crystalline orientations are studied for each phase: 1) Isotropic distribution: ZrO2m_iso; 2) Ideal fiber texture: ZrO2m_isoT/c3. For the monoclinic phase, the considered (001) fiber texture is the one observed for the oxide on nuclear fuel cladding, see Parise et al. (1998).

Voigt and Reuss Estimates of the Polycrystalline Thermo-Elastic Properties

The Voigt estimate of the effective thermo-elastic behavior of a polycrystal of Zirconia is obtained by assuming that the strain is homogeneous in the material. If $\varepsilon_{ij}{}^{g}$ are the components of the strain tensor in all the grains orientated in the g direction, then for all crystalline orientations g1, g2… gn we have:

$$\varepsilon_{ij}{}^{g1} = \varepsilon_{ij}{}^{g2} = \cdots = \varepsilon_{ij}{}^{gn} = E_{ij} \tag{4}$$

where E_{ij} are the components of the average strain tensor in the polycrystal, *i.e.* the "macroscopic" strain.

The components of the “macroscopic” stress $\sum_{ij}$ are obtained by averaging the stresses over all grain orientations *G*. If $C_{ijkl}{}^{g}$ are the components of the stiffness tensor of the grain oriented in the *g*

direction, then Equation 5 leads to the expression of the Voigt estimate C_{ijkl}^{V} of the polycrystal stiffness tensor, thanks to Equation 4.

$$\sum_{ij} = \frac{1}{G}\int_G \sigma_{ij}^{g}\,dg = \frac{1}{G}\int_G C_{ijkl}^{g} : \varepsilon_{kl}^{g}\,dg = \left(\frac{1}{G}\int_G C_{ijkl}^{g}\,dg\right) : E_{kl} = C_{ijkl}^{V} : E_{kl} \quad (5)$$

That leads to the expression of C_{ijkl}^{V}:

$$C_{ijkl}^{V} = \frac{1}{G}\int_G C_{ijkl}^{g}\,dg \quad (6)$$

Each crystalline orientation g is defined by 3 Euler angles $(\varphi_1, \emptyset, \varphi_2)$, see Engleret and Randle (2011), which relate the crystallophysic frame $(\vec{c}_1, \vec{c}_2, \vec{c}_3)$ to the global one $(\vec{x}, \vec{y}, \vec{z})$.

For a given crystalline orientation defined by $(\varphi_1, \emptyset, \varphi_2)$, the stiffness tensor C_{ijkl}^{g} expressed in the global frame is related to the stiffness tensor C_{ijkl}^{c} in the crystallophysic frame by the rotation matrix A_{ij}^{g} according to Equation 8.

$$C_{ijkl}^{\varphi_1,\emptyset,\varphi_2} = A_{ip}^{\varphi_1,\emptyset,\varphi_2} A_{jq}^{\varphi_1,\emptyset,\varphi_2} A_{km}^{\varphi_1,\emptyset,\varphi_2} A_{ln}^{\varphi_1,\emptyset,\varphi_2} C_{pqmn}^{c} \quad (8)$$

Noting $f(\varphi_1, \emptyset, \varphi_2)$ the density distribution function of Euler angles that defines the density distribution of crystalline orientations, dg is then equal to $f(\varphi_1, \emptyset, \varphi_2) d\varphi_1 . \sin\emptyset\, d\emptyset . d\varphi_2$ and Equations 6 and 8 lead to the expression of C_{ijkl}^{V} in Equation 9.

$$C_{ijkl}^{V} = \frac{1}{8\pi^2}\int_0^{2\pi} d\varphi_1 \int_0^{\pi} \sin\emptyset\, d\emptyset \int_0^{2\pi} A_{ip}^{\varphi_1,\emptyset,\varphi_2} A_{jq}^{\varphi_1,\emptyset,\varphi_2} A_{km}^{\varphi_1,\emptyset,\varphi_2} A_{ln}^{\varphi_1,\emptyset,\varphi_2} C_{pqmn}^{c} f(\varphi_1, \emptyset, \varphi_2) d\varphi_2 \quad (9)$$

Similarly, the Reuss estimate is obtained by assuming that the stress is homogeneous over the polycrystal. The same approach on the compliance tensor $S_{ijkl}^{g} = \left(C_{ijkl}^{g}\right)^{-1}$ leads to the Reuss estimate of the compliance tensor S_{ijkl}^{R} as expressed in Equation 10.

$$S_{ijkl}^{R} = \frac{1}{8\pi^2}\int_0^{2\pi} d\varphi_1 \int_0^{\pi} \sin\emptyset\, d\emptyset \int_0^{2\pi} A_{ip}^{\varphi_1,\emptyset,\varphi_2} A_{jq}^{\varphi_1,\emptyset,\varphi_2} A_{km}^{\varphi_1,\emptyset,\varphi_2} A_{ln}^{\varphi_1,\emptyset,\varphi_2} S_{pqmn}^{c} f(\varphi_1, \emptyset, \varphi_2) d\varphi_2 \quad (10)$$

Applying Equations 9 and 10, assessments of the moduli can be obtained according to the Voigt and Reuss bounds. In the case of an isotropic distribution of monoclinic zirconia, ZrO2m_iso, the Voigt bounds of the Young modulus is E_V=271 GPa and the Reuss bounds is E_R =226 GPa; the Poisson coefficient stemming from the Voigt estimate is ν_V=0.261 and that stemming from the Reuss estimate is ν_R=0.272. For a polycrystal of monoclinic zirconia with a fiber texture along the $\vec{c}_3$ axis (ZrO_2m_isoT/c3) these equations lead to the given values of C_{ijkl}^{V} and $C_{ijkl}^{R} = \left(S_{ijkl}^{R}\right)^{-1}$ given in the Equation 11 and that recovers the results of Parise et al. (1998).

$$C_{IJ}^{V}(\text{GPa}) = \begin{pmatrix} 395 & 141 & 97 & 0 & 0 & 0 \\ 141 & 395 & 97 & 0 & 0 & 0 \\ 97 & 97 & 240 & 0 & 0 & 0 \\ 0 & 0 & 0 & 127 & 0 & 0 \\ 0 & 0 & 0 & 0 & 89 & 0 \\ 0 & 0 & 0 & 0 & 0 & 89 \end{pmatrix} \quad C_{IJ}^{R}(\text{GPa}) = \begin{pmatrix} 374 & 156 & 93 & 0 & 0 & 0 \\ 156 & 374 & 93 & 0 & 0 & 0 \\ 93 & 93 & 219 & 0 & 0 & 0 \\ 0 & 0 & 0 & 109 & 0 & 0 \\ 0 & 0 & 0 & 0 & 75 & 0 \\ 0 & 0 & 0 & 0 & 0 & 75 \end{pmatrix} \quad (11)$$

In this case, the Young modulus in the x-direction is E_x^V=327 GPa and the Poisson ratio ν_{xy}^V=0.286 for the Voigt estimation, whereas for the Reuss estimation, ones finds E_x^R=294 GPa and ν_{xy}^V=0.348.

Thermal Expansion Ratio of Polycrystalline Zirconia

The coefficient of thermal expansion can be determined exactly for a given polycrystal texture in the frame of thermo-elasticity. For a fiber texture of monoclinic zirconia along the $\vec{c}_3$ axis (ZrO_2m_isoT/c3), the tensor of thermal expansion is given in Equation 12.

$$\alpha_{ij}\ (\times 10^{-6}\mathrm{K}^{-1}) = \begin{pmatrix} 4.57 & 0 & 0 \\ 0 & 4.57 & 0 \\ 0 & 0 & 12.78 \end{pmatrix} \tag{12}$$

Last, the coefficient of thermal expansion for isotropic distribution of crystalline orientations (ZrO2m_iso) is 7.3×10^{-6} K^{-1}.

ANALYSES AT A MACRO-SCALE

With the thermo-elastic properties of the oxide layer presented above, we developed a finite element model of the layer/substrate system to compute the stress state induced by a thermal expansion of zirconia. The goal is to compare these results to those usually obtained by analytical calculations.

Analytical Calculations

The analytical formulas currently used to assess residual stresses are derived from load balance within a plate with heterogeneous section. Moreover, the layer is supposed to be very thin, such that the substrate does no deform at all. The stress is induced by the mismatch in thermal expansion coefficients between the oxide and the substrate. For an oxide growing in the "z" direction and exhibiting isotropic properties, the stress induced by a temperature variation ΔT are given by the Equation 13, where E^f, ν^f, α^f are, respectively, the Young's modulus, the Poisson's ratio and the coefficient of thermal expansion of the film and α^s the coefficient of thermal expansion of the substrate.

$$\sigma_{xx}^f = \sigma_{yy}^f = \frac{E^f}{1-\nu^f}(\alpha^s - \alpha^f)\Delta T \tag{13}$$

If anisotropy is concerned, the stress is given by Equation 14:

$$\sigma_{xx}^f = \frac{{E_x}^f}{1-{\nu_{xy}}^f}(\alpha^s - {\alpha_{xx}}^f)\Delta T \tag{14}$$

$$\text{with}\quad {E_{xx}}^f = \frac{1}{{S_{xxxx}}^f} \quad {\nu_{xy}}^f = -\frac{{S_{xxyy}}^f}{{S_{xxxx}}^f} \tag{15}$$

where ${S_{ijkl}}^f$ is the compliance tensor of the layer.

Finite Element Model

The Figure 1 presents the mesh of the layer/substrate system. The modeling is achieved with Cast3M, the finite element software developed by the CEA (see CEA). The finite elements are linear hexahedra. The substrate dimensions are 10mm×10mm×0.5mm, whereas the layer dimensions are 10mm×10mm×0.002mm. This layer thickness is approximately the value at which lateral cracking and breakdown in oxidation occur, as recalled by Motta et al. (2007) for example. The substrate has the thermo-elastic properties of Zircaloy-4: E=80 GPa, ν=0.3 and $\alpha=7.4\times10^{-6}$ K^{-1}. Since the mechanical behavior gets the same symmetry as the geometry, symmetry of the displacements is prescribed along the

planes $(A, \vec{x}, \vec{z})$ and $(A, \vec{y}, \vec{z})$ and point A is blocked $(\vec{u}(A) = \vec{0})$, that defines one quarter of the actual geometry. With such boundary conditions, curvature of the system may develop, modifying the stress distribution. We prescribe an arbitrary temperature variation of -100°C. The stress level for an expansion magnitude equivalent to the one developed by oxide growth can be post-processed from this loading, thanks to linear elasticity, as long as the hypothesis of linear behavior remains correct, in particular for the substrate.

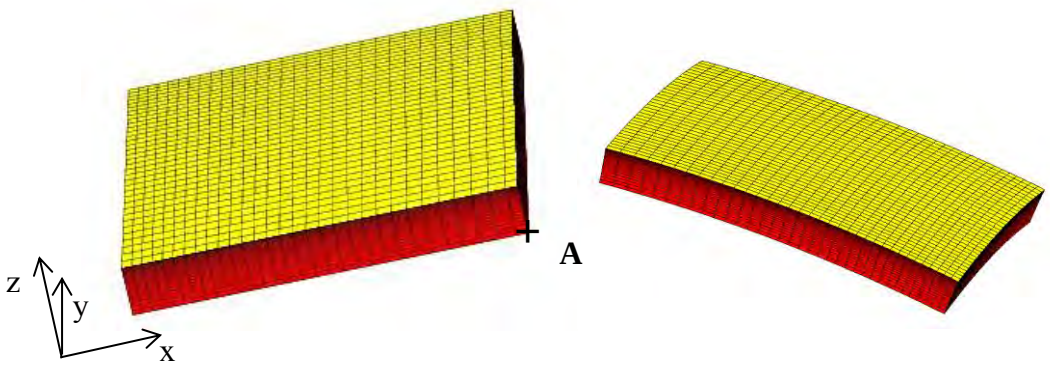

Figure 1. left: mesh of the layer (yellow)/substrate (red) system modeled; right: deformed ×500.

Results

The Table 1 presents the results derived either from FE and analytical calculations on the stress induced in the layer by an arbitrary temperature variation of -100°C. One can verify that the analytical calculations match very well the FE results if the anisotropy of the layer is taken into account. But on the contrary, if the stress level is estimated by considering the layer as isotropic when it is not, the error can be then very large. It is therefore important to take into account the anisotropy of the layer when calculating the residual stress in an oxide/layer system. It should be noted that the curvature is negligible in the stress assessment because the layer thickness is small. If the thickness increases, the Equations 13 or 14 are no more valid.

Table 1: Stress level in the oxide layer induced by an arbitrary temperature variation of -100°C according to different hypothesis of the layer polycrystalline microstructure and with the Voigt estimates.

Polycrystalline microstructure	Numerical results (MPa)	Analytical calculations (MPa)	
		Isotropic	Anisotropic
ZrO2m_iso	-3.5	-3.6	-3.6
ZrO2m_isoT/c3	-121.1		-121.5

ANALYSES AT MICRO-SCALE

The analyses here above were achieved under the classical consideration that the oxide layer is homogeneous, even if we take into account its crystallographic microstructure through its mechanical behavior. In this section, we use linear tetraahedra to mesh Voronoï polyhedrons which represent the polycrystalline microstructure of the layer. With these models, we aim at studying three points. First, we compute the effective thermo-elastic properties of aggregates to better assess the modulus tensor than

with the Voigt and Reuss estimates. Second, we analyze the intragranular stress distribution over the aggregates according to different hypothesis on the crystallographic texture of the oxide. Last, we also study the influence of the grain morphology, equiaxed vs. columnar; on the stress distribution over the aggregate.

Microstructure modeling

The Figure 2 illustrates different meshes of Voronoï polyhedrons used to model the polycrystalline microstructure of the layer. These meshes were achieved with Cast3M, as the following computations. These pictures only show the edges of the grains, which are also arbitrarily colored to be more easily distinguished. Each grain behaves as a crystal of monoclinic zirconia which orientation is defined by 3 Euler angles for the isotropic texture and by only one for the fiber texture. These angles are randomly determined by a Monte-Carlo process from a uniform distribution. In this study, we used 5 meshes of 64 grains and 2 meshes of 512 grains to analyze the influence of the grain number per mesh on the results. We also studied the influence of the mesh refinement by refining a 64 grains mesh (496,170 elements for the fine mesh density vs. 61,845 for the basic mesh density). Elongated polyhedrons were generated in order to study the influence of the morphological texture on intragranular stresses. All these meshes are made up of linear tetrahedrons.

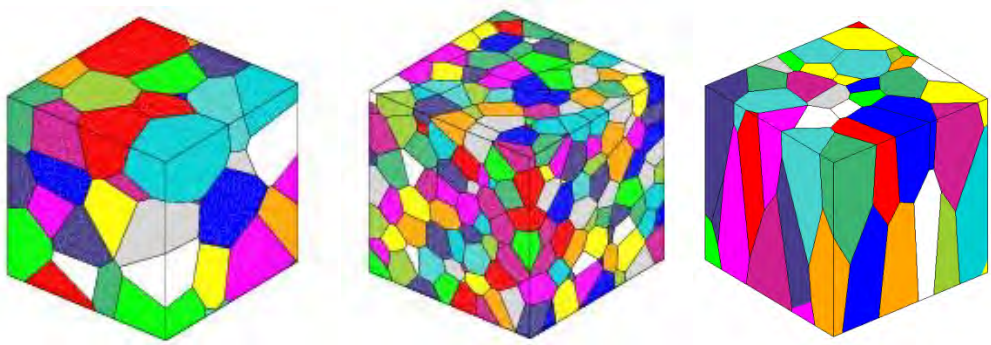

Figure 3. Different meshes of Voronoï polyhedrons: mesh with 64 grains (left), meshes with 512 grains (middle) and with 74 elongated grains (right).

Thermo-elastic properties

First we determine the elastic properties of the polycristalline aggregates by prescribing Kinematic Uniform Boundary Conditions (KUBC), defined by Equation 20.

$$\vec{u} = \bar{\bar{\varepsilon}} \cdot \vec{x} \tag{16}$$

where $\vec{u}$ is the displacement of a point $\vec{x}$ on the mesh boundary and $\bar{\bar{\varepsilon}}$ is a constant strain tensor.

In order to get all the components of the stiffness tensor, we compute the mean value of the stress components for 6 elementary loadings, 3 extensions in the $\vec{x}$, $\vec{y}$ and $\vec{z}$ directions, and 3 glides of the planes orthogonal to these directions. Equation 17 illustrates how we get the components of the first column of the stiffness tensor by applying a pure extension loading of magnitude ε^0 in the $\vec{x}$ direction. The expression of $< \sigma_I{}^x >_v$ is given in Equation 18, where V is the volume of the mesh while the subscript x is related to the global frame.

$$\begin{bmatrix} <\sigma_{xx}> \\ <\sigma_{yy}> \\ <\sigma_{zz}> \\ <\sigma_{xy}> \\ <\sigma_{xz}> \\ <\sigma_{yz}> \end{bmatrix} = \begin{bmatrix} <\sigma_1> \\ <\sigma_2> \\ <\sigma_3> \\ <\sigma_4> \\ <\sigma_5> \\ <\sigma_6> \end{bmatrix} = \begin{bmatrix} C_{11} & C_{12} & C_{13} & C_{14} & C_{15} & C_{16} \\ C_{21} & C_{22} & C_{23} & C_{24} & C_{25} & C_{26} \\ C_{31} & C_{32} & C_{33} & C_{34} & C_{35} & C_{36} \\ C_{41} & C_{42} & C_{43} & C_{44} & C_{45} & C_{46} \\ C_{51} & C_{52} & C_{53} & C_{54} & C_{55} & C_{56} \\ C_{61} & C_{62} & C_{63} & C_{64} & C_{65} & C_{66} \end{bmatrix} \begin{bmatrix} \varepsilon^0 \\ 0 \\ 0 \\ 0 \\ 0 \\ 0 \end{bmatrix} \quad \rightarrow \quad {C_{IJ}}^x = \frac{<{\sigma_I}^x>_v}{\varepsilon^0} \tag{17}$$

$$<\sigma_{ij}>_V = \frac{1}{V}\int \sigma_{ij} dV \tag{18}$$

Static uniform boundary conditions are also applied following the same procedure as below except that uniform pressure is applied on each face of the VE and that 6 degrees of freedom are blocked in order to avoid any rigid body motion.

Equations 19 and 20 present typical values of the components of the stiffness tensor we obtained on a mesh with 512 grains and the fiber texture of monoclinic zirconia for kinematic uniform boundary conditions (KUBC) and static uniform boundary conditions (SUBC). The tensor is symmetric but some values that should be zero are not due to some boundary effects (the values set to 0 are inferior to 0.1 GPa). The moduli computed on meshes with 64 grains are stiffer, as expected. But the relative difference with the results on meshes with 512 grains is lower than 4% on all the components. Moreover, the highest relative difference between the moduli obtained on the two meshes with 512 grains is lower than 1%.

$${C_{IJ}}^{KUBC}(GPa) = \begin{pmatrix} 387 & 146 & 95 & 0 & 0 & 1.2 \\ 146 & 389 & 97 & 0 & 0 & -1.8 \\ 95 & 97 & 234 & 0 & 0 & 0 \\ 0 & 0 & 0 & 121 & 1.4 & 0 \\ 0 & 0 & 0 & 1.4 & 84 & 0 \\ 1.2 & -1.8 & 0 & 0 & 0 & 84 \end{pmatrix} \tag{19}$$

$${C_{IJ}}^{SUBC}(GPa) = \begin{pmatrix} 384 & 149 & 95 & 0 & 0 & 1.1 \\ 146 & 386 & 96 & 0 & 0 & -1.7 \\ 95 & 97 & 231 & 0 & 0 & 0 \\ 0 & 0 & 0 & 118 & 1.5 & 0 \\ 0 & 0 & 0 & 1.5 & 81 & 0 \\ 1.1 & -1.7 & 0 & 0 & 0 & 81 \end{pmatrix} \tag{20}$$

The computed values of the stiffness tensors are well framed by the Voigt and Reuss bounds. Furthermore, KUBC and SUBC lead to very close estimates. So, the Volume Element of 512 grains can be considered as representative of the textured, monoclinic zirconia for elastic properties. It is worth noting that the element volume composed of 64 grains give similar results.

We also determine the coefficient of thermal expansion by computing the mean value of the strain components under a pure thermal loading $\Delta T = -100°C$ of arbitrary magnitude, as expressed in Equation 21. In this case, we only block 6 degrees of freedom to avoid any rigid body motion, with 6 free surfaces.

$${\alpha_{ij}}^x = \frac{<{\varepsilon_{ij}}^x>_v}{\Delta T} \tag{21}$$

Results obtained on the 512g1 mesh are given in Table 1 for the different crystallographic textures. As one can see, the values are very close to those expected theoretically, that confirms that the results obtained on the meshes with 512 grains are relevant.

Table 1. Coefficients of thermal expansion computed with the 512 grains mesh for the different textures of the oxide layer and comparisons with the theoretical values.

	Numerical (K^{-1})			Theory (K^{-1})		
	α_{11}	α_{22}	α_{33}	α_{11}	α_{22}	α_{33}
ZrO2m_iso	6.68E-06	6.99E-06	7.04E-06	7.3E-06		
ZrO2m_isoT/c3	4.61E-06	4.47E-06	12.5E-06	4.57E-06	4.57E-06	12.7E-06

Influence of the Crystallographic and Morphological Texture on the Intra-granular Stress State

Figure 3 presents the distribution density of the σ_{xx} stress component in the 512 grains mesh for the different crystallographic textures under an extension in the $\vec{x}$ direction (right curves). The picture on the left illustrates the computed stress fields. In the case of an ideal fiber texture of monoclinic zirconia (ZrO2t_isoT/c3), the stress distribution density is modified compared to that obtained assuming isotropic texture (ZrO2m_iso): the value of the mean stress is shifted to higher values and the dispersion is much lower. For both crystallographic textures, the stress can reach 450 MPa in some elements, but the mean value is 388 MPa for the fiber texture and only 256 MPa for the isotropic distribution.

We also considered elongated grains associated with the fiber texture: the shape of the grains does not modify the stress distribution. As a matter of fact, the stress distribution only depends on the distribution function of crystalline orientations.

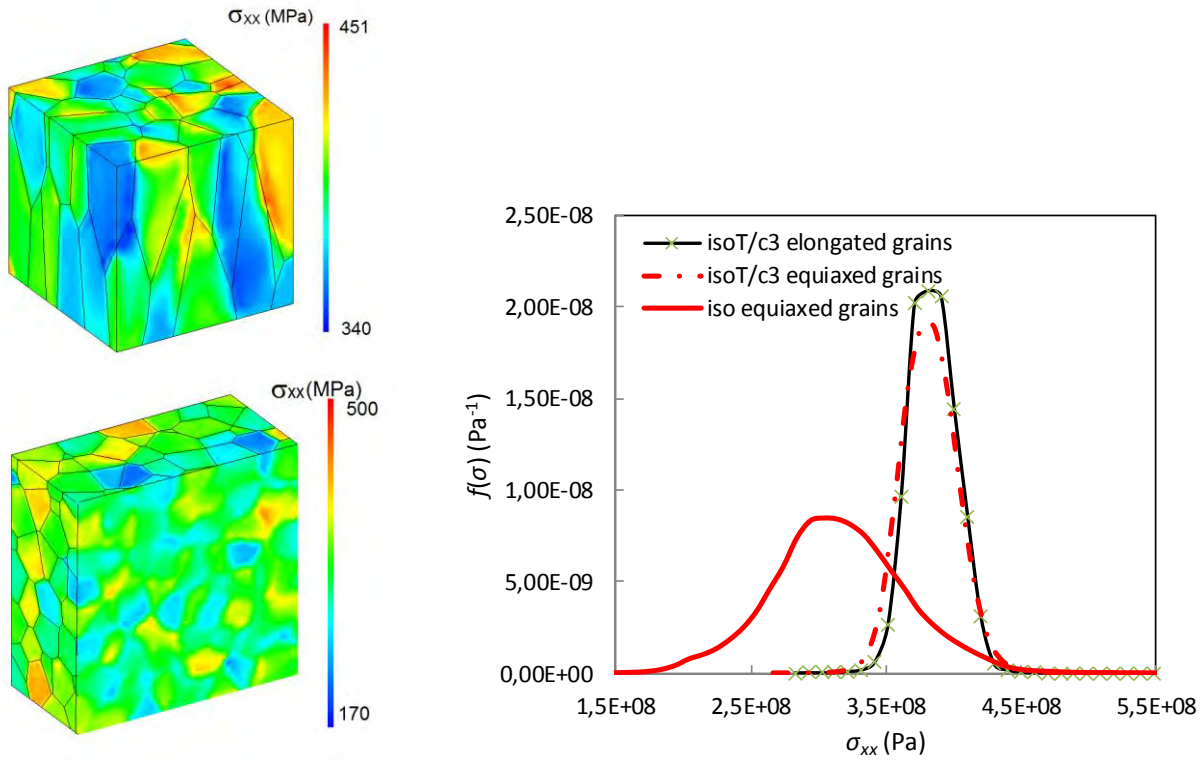

Figure 3. Extension in the x-direction (ε^0=0.001). Left: σ_{xx} isovalues computed at gauss points for ZrO2m_iso within the volume cut by a plane perpendicular to the x-direction. Right: distribution densities for crystallographic textures and morphological textures (512 grains).

Figure 4 presents the isovalues of the σ_{xx} stress component and the distribution densities of the σ_{xx} and σ_{zz} stress components for the fiber texture under a thermal loading of $\Delta T = -100°C$ (prescribed fiber texture induces a transversely isotropic behavior in the global (x, y, z) coordinate system, so that $\sigma_{xx} = \sigma_{yy}$ at the macroscale and the distributions of these stresses are identical). Since the thermal expansion is anisotropic at the crystalline scale, homogeneous thermal loading induces internal stresses inside the polycrystal. The component related to the fiber axis σ_{zz}, is less dispersed than the component σ_{xx}. Considering that the substrate prevents the thermal expansion of the layer, the layer will be submitted to compression. So, the stress distribution density in a layer submitted to a thermal loading will be a composition of the one stemming from mechanical loading and the one stemming from free thermal loading. It is worth noting that for the free thermal loading of only -100°C, microscopic stress can reach 80-100 MPa.

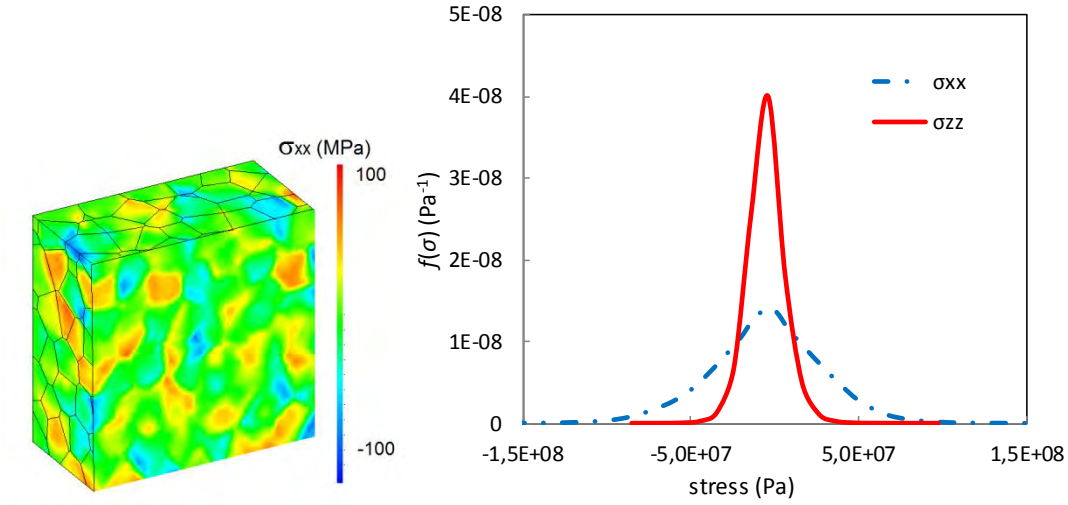

Figure 4. Thermal expansion (ΔT=-100°C). Left: σ_{xx} isovalues for ZrO2m_isoT/c3. Right: distribution densities of the σ_{xx} and σ_{zz} stress components (512 grains).

CONCLUSIONS

First, the comparisons between the computations achieved at the layer/substrate system scale and the results given by the analytical formulas commonly used to derive the residual stresses from strain measurements are in good agreement as long as the assumptions on the thermo-elastic properties of the oxide layer remain valid. If not, the residual stress evaluated with these formulas may be very different from what have been computed.

Second, computations on VE gave accurate estimates of the effective properties of the polycrystalline aggregates of zirconia. From all the investigations we achieved on the thermo-elastic properties on these polycrystalline aggregates, we can consider that the meshes with 512 grains accurately represent the effective behavior of the oxide layer.

These computations also confirmed the influence of the crystallographic texture on the mechanical behavior of the oxide layer, but showed no influence of the morphological one. Last, the analysis of the intragranular stress distribution showed that the maximal stress may be 30% higher than its mean value in the layer in the case of isotropic distribution and about 13% higher than its mean value in the case of textured zirconia. The anisotropy of the expansion coefficient induces an additional scatter of the intragranular stress. This stress distribution at microscopic scale should be integrated to the failure analysis of the zirconium oxide layers.

ONGOING STUDIES

This paper have presented the status of ongoing studies on the intragranular stress state in the layer/substrate systems, in particular the systems defined by oxidized zirconium alloys commonly used in nuclear reactor. With a help of meshes of Voronoï polyhedrons to model a Volume Element of the layer microstructure, we are working now to model the system with loadings and boundary conditions more relevant, which means:

1) To take into account the influence of the substrate on the mechanical responser of the layer,
2) To apply the self-equilibrated stress state induced by oxide growing on the system.

The first point is achieved by embedding the Volume Element in a larger mesh which models the layer/substrate system. One face of the Volume Element is placed at the interface between the layer and the substrate and the 5 other faces are surrounded by the mesh of the layer. For the second point, we simply apply the stress state given by the analytical formulas of the shell theory by using kinematic or static uniform boundary conditions on the global mesh. However, new questions appear in this way. Due to the difference of size between the grains of the layer (some 10^{th} of nanometers) and the substrate (some 10^{th} of micrometers), the volume underneath the Volume Element of the oxide layer only represents one grain or, at most, 3 grains at a grain boundary. In this case, the crystallographic orientation of the substrate may strongly influence the results on the Volume Element.

REFERENCES

Benali, B., Herbst Ghysel, M., Gallet, I., Huntz, A.M. and Andrieux, M. (2006). "Stress driven phase transformation in ZrO2 film", *Appl. Surf. Sc.*, 253, 1222–1226.

Berdin, C., YAO, Z.Y. and Pascal, S. (2013). "Internal stresses in polycrystalline zirconia: microstructure effects," *Comp. Mat. Sc.*, 70, 140-144.

Bernard, O., Huntz, A. M., Andrieux, M., Seiler, W., Ji, V. and Poissonnet, S. (2007). "Synthesis, structure, microstructure and mechanical characteristics of MOCVD deposited zirconia films," *Appl. Surf. Sc.*, 253, 4626–4640.

CEA, DEN, DM2S, SEMT, Cast3M, http://www-cast3m.cea.fr

Chen, Z., Prud'homme, N., Wang, B. and Ji,, V. (2011). "Residual stress gradient analysis with GIXRD on ZrO2 thin films deposited by MOCVD," *Surf. and Coat. Tech.*, 206, 405–410.

Engleret, O. and Randle V. (2011). *Introduction to texture analysis, 2nd ed.*, CRC Press.

Motta, A.T., Yilmazbayhan, A., Gomes Da Silva, M.J., Comstock, R.J., Was, G.S., Busby, E., Gartner, J.T., Peng, Q., Jeong, Y. H. and Park, J.Y. (2007). "Zirconium alloys for supercritical water reactor applications: challenges and possibilities", *J. Nucl. Mat.*, 371, 61-75.

Parise, M., Sicardy, O. and Cailletaud, G., (1998). "Modelling of the mechanical behavior of the metal-oxide system during Zr alloy oxidation," *J. Nuc. Mat.*, 256, 35-46.

Simeone, D., Baldinozzi, G., Gosset, D., Dutheil, M., Bulou, A. and Hansen, T., (2003). "Monoclinic to tetragonal semi-reconstructive phase transition of zirconia," *Phys. Rev. B*, 67, 1-7.

Zhao, X., Li Shang, S., Liu, Z.K. and Shen, J.Y. (2011). "Elastic properties of cubic, tetragonal and monoclinic ZrO2 from first-principles calculations," *J. of Nuc. Mat.*, 415, 13–17.